Available online at www.sciencedirect.com
SCIENCE DIRECT®
Journal of Molecular Structure 695–696 (2004) 253–261
Journal of MOLECULAR STRUCTURE
www.elsevier.com/locate/molstruc

A theoretical study of the millimeterwave spectrum of CH_5^+

P.R. Bunker*, B. Ostojić, S. Yurchenko

Steacie Institute for Molecular Sciences, National Research Council of Canada, Ottawa, Ont., Canada K1A 0R6

Received 27 October 2003; revised 16 December 2003; accepted 16 December 2003

Abstract

This is a continuation of our earlier work aimed at predicting the millimeterwave spectrum of protonated methane CH_5^+. As for protonated acetylene $C_2H_3^+$, it is the millimeterwave spectrum that will most directly provide the experimental information needed to understand the large amplitude motion of the molecule. Literature ab initio calculations show that the large amplitude motion of the five protons around the central carbon nucleus in CH_5^+ is not completely free, but is restricted by potential barriers at the trigonal bipyramid (D_{3h}), square pyramid (C_{4v}) and end-on-H_2 (C_{3v}) forms. Thus, the large amplitude motion proceeds mostly in the coordinate space that connects the structures called C_s(I), C_s(II) and C_{2v}. These structures have essentially identical electronic energies and very similar rotational constants, as has already been shown in the literature. We calculate that they also have very similar dipole moments. The topology of the space of the large amplitude motion that connects the 120 versions of the C_s(I) structure, the 120 versions of the C_s(II) structure, and the 60 versions of the C_{2v} structure is considered here. The spectral signature of this large amplitude motion in the rotational spectrum is calculated with absolute intensities. It is hoped that these results will aid and stimulate attempts to see and assign the high resolution gas phase millimeterwave absorption spectrum of CH_5^+. The $J = 1 \leftarrow 0$ spectrum is predicted to be centered in the region 220–235 GHz, and if all the large amplitude motion splittings of this line are resolved, the strongest component (the $K_i = 0 \leftarrow 0$ line) is predicted to have an integrated absorption intensity of 13 m/mol at 77 K.

Keywords: Theory; Protonated methane; High-resolution spectroscopy

1. Introduction

It is more than 50 years since Talroze and Lyubimova [1] reported a mass-spectroscopic study of the production of CH_5^+ in the reaction

$$CH_4^+ + CH_4 \rightarrow CH_5^+ + CH_3, \quad (1)$$

and their work marks the beginning of the systematic study of ion-molecule reactions in the gas phase. In the intervening years, there have been many experimental studies of this reaction (see, for example, Ref. [2] and references therein). In studies of methane in solution under superacid conditions evidence has been obtained by Olah and colleagues that CH_5^+ is formed and that it is very short lived in this environment, releasing H_2 and oligomerizing with more methane (see Ref. [3] for a recent review). As a small molecule with few electrons, it has also been the subject of numerous ab initio calculations of which Refs. [4–6] are examples. The calculations show that the molecule will have large amplitude internal motions with low hindering barriers, but these have yet to be spectroscopically characterized.

We know a great deal about how to make this ion and about how it reacts. However, no assigned high-resolution gas phase spectrum of CH_5^+ has been obtained. To probe the large amplitude tunneling motions it is best to look at the molecular spectrum in the appropriate long wavelength region. Thus, the purpose of this paper is to motivate a search in the millimeterwave region of the spectrum, and to provide some help in the recognition and assignment of such a spectrum once it has been obtained. As pointed out for $C_2H_3^+$ in Ref. [7] (see also Section 3 of [8]), the 3 μm region of the spectrum (probably observed for CH_5^+ in Ref. [9]) will be riddled with perturbations from underlying dark states, and this will preclude the analysis of the spectral splittings in terms of only the large amplitude motion dynamics. Based on the experience with $C_2H_3^+$ from Ref. [10], it is surely best to start with the millimeterwave spectrum.

* Corresponding author. Tel.: +1-613-9900738; fax: +1-613-9472838.
E-mail address: philip.bunker@nrc.ca (P.R. Bunker).

0022-2860/$ - see front matter © 2003 Elsevier B.V. All rights reserved.
doi:10.1016/j.molstruc.2003.12.020

2. The topology of the proton motion

Fig. 1 shows the structures of the six important stationary point isomers of CH_5^+ that are the subject of the ab initio calculations reported by Schleyer and Carneiro [4]. The structures **1** though **6** are called the C_s(I), C_s(II), C_{2v}, C_{4v}, D_{3h} and C_{3v} structures, respectively. With geometry optimization, the energies of these six structures were obtained as a function of basis set and ab initio method in Ref. [4]. As a result, it was found that structure **1** is minimum on the surface and that the other five structures are saddle points. Inclusion of the zero-point energies for the higher frequency vibrational modes gives structures **1**–**3** essentially the same energy, whereas the structures **4**–**6** have energies that are about 1, 10 and 30 kcal/mol higher, respectively. The dissociation energy $D(CH_3^+-H_2)$ was obtained as 42 kcal/mol. More recent, higher level ab initio calculations [5,6] have not changed these general results. Disregarding the possibility of the molecule deforming through structures **4**–**6**, we can understand the topology of the large amplitude motion by only focusing on the motions that take us through structures **1**–**3**, and all versions of them. Versions are structures that only differ in the way the protons are labeled [11].

Structures C_s(I) and C_s(II) interconvert via internal rotation of the H_2 and CH_3 moieties relative to each other. In Fig. 2, we show two versions of the C_s(I) structure that internally rotate through a version of the C_s(II) structure. In the versions depicted in Fig. 2, the H_2 moiety has its protons numbered 1 and 2, and viewed from the H_2 end the proton numbering on the CH_3 moiety increases in the clockwise 'c' direction; as a result we identify these versions as being based on what we call the '12c form' of CH_5^+. We denote the actual versions of the C_s(I) structure depicted in Fig. 2(a) and (b) as 12c[13] and 12c[25], respectively, where the numbers in the square brackets denote which protons of the H_2 and CH_3 moieties eclipse each other. The (12)c form can internally rotate through six versions of the C_s(I) structure which we can represent as

$$(12)c[13] \rightarrow 12c[25] \rightarrow 12c[14] \rightarrow 12c[23] \rightarrow 12c[15] \rightarrow 12c[24] \rightarrow 12c[13]. \quad (2)$$

There are 10 ways of choosing the two protons that form the H_2 moiety and for each of these the remaining three protons can be arranged so that the labeling numbers increase in the clockwise 'c' or anticlockwise 'a' direction. Thus, there are 20 forms of the molecule, such as 12c, 12a, 13c, 13a, etc. each of which can internally rotate through six versions of the C_s(I) structure. This means that there are 120 versions of the C_s(I) structure, and these can be organized into 20 sets of six within which internal rotation motion takes place; this is done in Table 1. Obviously, there are also 120 versions of the C_s(II) structure.

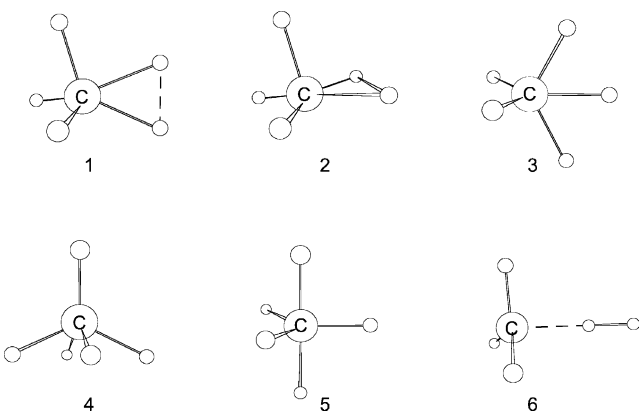

Fig. 1. The six isomers of CH_5^+ considered in Ref. [4].

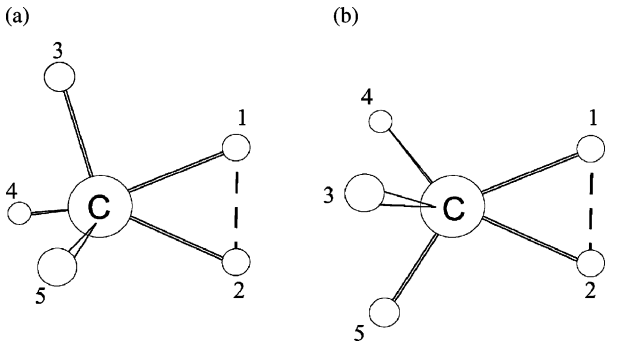

Fig. 2. Two versions of the C_s(I) structure that interconvert by internal rotation via a version of the C_s(II) structure.

Table 1
The 120 versions of the C_s(I) structure of CH_5^+ arranged in horizontal rows connected by the internal rotation motion

12c[13]	12c[25]	12c[14]	12c[23]	12c[15]	12c[24]
12a[13]	12a[24]	12a[15]	12a[23]	12a[14]	12a[25]
13c[12]	13c[35]	13c[14]	13c[32]	13c[15]	13c[34]
13a[12]	13a[34]	13a[15]	13a[32]	13a[14]	13a[35]
14c[12]	14c[45]	14c[13]	14c[42]	14c[15]	14c[43]
14a[12]	14a[43]	14a[15]	14a[42]	14a[13]	14a[45]
15c[12]	15c[54]	15c[13]	15c[52]	15c[14]	15c[53]
15a[12]	15a[53]	15a[14]	15a[52]	15a[13]	15a[54]
23c[21]	23c[35]	23c[24]	23c[31]	23c[25]	23c[34]
23a[21]	23a[34]	23a[25]	23a[31]	23a[24]	23a[35]
24c[21]	24c[45]	24c[23]	24c[41]	24c[25]	24c[43]
24a[21]	24a[43]	24a[25]	24a[41]	24a[23]	24a[45]
25c[21]	25c[54]	25c[23]	25c[51]	25c[24]	25c[53]
25a[21]	25a[53]	25a[24]	25a[51]	25a[23]	25a[54]
34c[31]	34c[45]	34c[32]	34c[41]	34c[35]	34c[42]
34a[31]	34a[42]	34a[35]	34a[41]	34a[32]	34a[45]
35c[31]	35c[54]	35c[32]	35c[51]	35c[34]	35c[52]
35a[31]	35a[52]	35a[34]	35a[51]	35a[32]	35a[54]
45c[41]	45c[53]	45c[42]	45c[51]	45c[43]	45c[51]
45a[41]	45a[52]	45a[43]	45a[51]	45a[42]	45a[53]

Each row represents one of the 20 possible internally rotating forms of the structure such as 12c, 12a, 13c, etc. (see text), and each entry represents one of the six versions of that form such as 12c[13], 12c[25], 12c[14], etc. (see text).

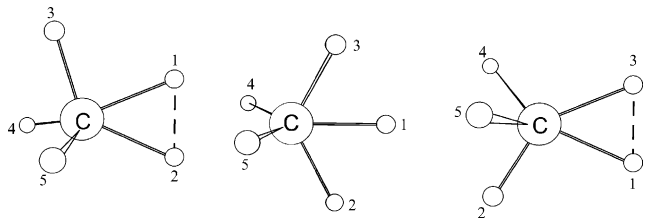

Fig. 3. Two versions of the C_s(I) structure that interconvert by a flip, and the version of the C_{2v} structure that connects them.

There are 60 versions of the C_{2v} structure, and in Fig. 3 we show how the versions 12c[13] and 13a[12] of the C_s(I) structure are connected by one of the versions of the C_{2v} structure. We call this motion a 'flip'. The 60 versions of the C_{2v} structure connect the 120 versions of the C_s(I) structure in pairs. These connected pairs are shown in Table 2.

In Table 1, one could now draw in each of the 60 flip connections from Table 2. In the true space of the vibrational motions each of these connections has the same 'length' and involves passing through a C_{2v} structure. Thus, from the ab initio results we infer that the molecule undergoes motion between all 120 versions of the C_s(I) structure, all 120 versions of the C_s(II) structure, and all 60 versions of the C_{2v} structure via two types of connection: internal rotation and the flip. If we knew the effective (zero-point averaged) structure and energy along the internal rotation and flip paths we would have all the information required to quantify the motion along each path. In principle, this would seem to be a two-dimensional (2D) problem, if we can introduce two appropriate dynamical variables that 'move' the molecule along each path.

To understand what we mean by 'appropriate dynamical variables' think of the HF dimer, in which there is an analogous problem in only one-dimensional (1D) [12]. For the HF dimer, there is a 1D minimum energy 'valley' through the 6D potential energy surface, and the molecule can be 'made to move' along the minimum energy valley, and the Schrödinger equation set up and solved for motion along that path, by introducing a single dynamical variable (called ρ); the other coordinates, and the potential energy function, are expressed as functions of ρ. The dynamical variable ρ is defined to be $(\theta_1 + \theta_2)/2$ where θ_1 and θ_2 are the angles between the HF axes and the line joining their centers of mass. The key feature of the work is the introduction of the coordinate $\sigma = (\theta_1 - \theta_2)/2$ as a *function* of ρ. The angle σ is not a dynamical variable in the calculation, but it occurs in equations that define the molecular structure. With a suitable definition of σ as a function of ρ, we can arrange that as ρ changes the angles θ_1 and θ_2 each change so that the molecule moves along the valley minimum in the potential surface. Section II of Ref. [12] explains the details (see, in particular Eqs. (1)–(5) and Table 1 in Ref. [12]).

One needs analytical expressions for two appropriate dynamical variables, ρ_1 and ρ_2 say, as functions of the HCH bond angles and HCaH dihedral angles (where 'a' is the center of mass of the H_2 moiety) in CH_5^+. One would also need expressions for the bond lengths and other angles as functions of ρ_1 and ρ_2 in order that changes in ρ_1 and ρ_2 would drive the molecule along the pathways connecting all versions of the C_s(I), C_s(II) and C_{2v} structures. Using an effective potential energy function of ρ_1 and ρ_2, one could then set up the appropriate 2D HBJ Hamiltonian [13–15] and solve it for the large amplitude motion.

In lieu of this approach, which has not yet been implemented, we have previously described a 120×120 matrix diagonalization approach [16–19]; see, in particular, Section IV of [17]. We use this matrix diagonalization approach again here in a calculation of the millimeterwave spectrum with a quantitative evaluation of line intensities. The effect on the energy levels and the spectrum of varying the relative energies of the C_s(I), C_s(II) and C_{2v} structures is also considered. Before presenting these results, we first describe some ab initio calculations of energies, structures and dipole moments.

3. The ab initio calculations

To satisfy ourselves about the structure and energy of the optimum (equilibrium) CH_5^+ form as a function of ab initio basis set size, we have used the MOLPRO program system

Table 2
The 60 pairs of versions of the C_s(I) structure of CH_5^+ that are connected through a C_{2v} flip transition state

12c[13]–13a[12]	12c[25]–25a[21]	13c[35]–35a[31]	14c[45]–45a[41]	15c[54]–45a[51]
12c[14]–14c[12]	12c[23]–23a[21]	13c[32]–23a[31]	14c[42]–24a[41]	15c[52]–25a[51]
12c[15]–15a[12]	12c[24]–24c[21]	13c[34]–34c[31]	14c[43]–34c[41]	15c[53]–35c[51]
12a[13]–13c[12]	12a[24]–24a[21]	13a[34]–34a[31]	14a[43]–34a[41]	15a[53]–35a[51]
12a[15]–15c[12]	12a[23]–23c[21]	13a[32]–23c[31]	14a[42]–24c[41]	15a[52]–25c[51]
12a[14]–14a[12]	12a[25]–25c[21]	13a[35]–35c[31]	14a[45]–45c[41]	15a[54]–45c[51]
13c[14]–14a[13]	23c[24]–24a[23]	23c[35]–35c[32]	24c[45]–45c[42]	25c[54]–45c[52]
13c[15]–15c[13]	23c[25]–25c[23]	23c[34]–34a[32]	24c[43]–34a[42]	25c[53]–35a[52]
13a[15]–15a[13]	23a[25]–25a[23]	23a[34]–34c[32]	24a[43]–34c[42]	25a[53]–35c[52]
13a[14]–14c[13]	23a[24]–24c[23]	23a[35]–35a[32]	24a[45]–45a[42]	25a[54]–45a[52]
14c[15]–15a[14]	24a[25]–25a[24]	34c[35]–35a[34]	34c[45]–45a[43]	35c[54]–45a[53]
14a[15]–15c[14]	24a[25]–25c[24]	34a[35]–35c[34]	34a[45]–45c[43]	35a[54]–45c[53]

Each of the five columns contains 12 pairs of such connections that are topologically related.

Table 3
The results of optimized CCSD(T) ab initio structure calculations for the C_s(I) form, using cc-pVnZ basis with $n = 2$–4

n	Energy, E_h	A_e (GHz)	B_e (GHz)	C_e (GHz)
2	−40.6031397	130.0	113.2	107.5
3	−40.6676705	133.9	116.3	110.3
4	−40.6934391	134.0	116.6	110.6

[20] to make optimized CCSD(T) calculations with a series of successively larger basis sets. We have used Dunning's correlation-consistent Gaussian basis sets cc-pVnZ with $n = 2$–4 [21]. Consistent with other earlier high level optimized ab initio results [4,5], we find the C_s(I) form to be the minimum energy structure. In Table 3, we show how the energy and equilibrium rotational constants converge as n is increased in these calculations. The largest basis set used ($n = 4$) has the AO contractions C(l2s6p3d2f1g/5s4p3d2f1g) and H(6s3p2d1f/4s3p2d1f).

The $J = 1 \leftarrow 0$ rotational transition will be centered around the position of $2\bar{B}_0 = B_0 + C_0$, and will have tunneling fine structure characteristic of the large amplitude motion discussed in Section 2. As can be seen from Table 3, our calculation yields a rather well converged value of $2\bar{B}_e = 227.2$ GHz. The CCSD(T)/TZ2P + f calculations in Ref. [5] are nearly at the level of our CCSD(T) $n = 3$ ab initio calculation, and they find $2\bar{B}_e$ to have the values 224.3, 223.9 and 232.3 GHz for the optimum C_s(I), C_s(II) and C_{2v} structures, respectively. The large amplitude motion will average out these values. In Ref. [19], the effect of the small amplitude vibrations was considered, and it was determined in an ab initio calculation, by summing the $\alpha/2$ corrections for the 11 modes (excepting the torsional mode), that

$$\bar{B}_0 = 0.9995\bar{B}_e, \tag{3}$$

which is a correction of −0.1 GHz to $2\bar{B}_e$. It was further determined in Ref. [19] that $D_J = 2$ MHz. Thus, on the basis of all these considerations we can expect that the $J = 1 \leftarrow 0$ rotational transition in CH_5^+ will be centered in the region of 220–235 GHz.

It is important to have an estimate of the absolute intensity of the rotational spectrum, and we have used the program system GAUSSIAN 98 [22] to calculate the dipole moments of the optimized C_s(I), C_s(II) and C_{2v} structures. We use the optimized geometries from Ref. [5] since they are all obtained at the same level of ab initio method. To calculate the dipole moments at these geometries, we use the CCSD(T) method with a cc-pVQZ basis set (i.e. $n = 4$ in the above notation). We obtain dipole moments of 1.6, 1.6 and 1.5 D for the C_s(I), C_s(II) and C_{2v} structures, respectively. By this time, the reader will have realized that these three structures are not very different from each other; they have very similar electronic energies, rotational constants and dipole moments.

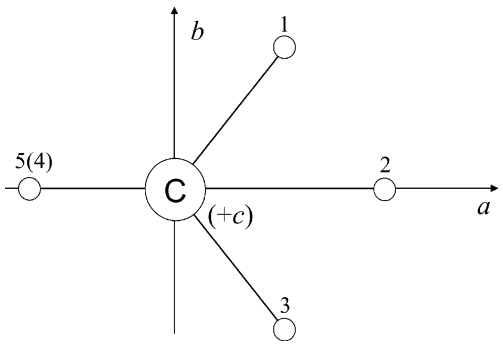

Fig. 4. A version of the C_{2v} structure.

4. Energy level correlations

Before giving the results of the quantitative calculations, it is helpful to consider the correlation diagram connecting the rotation and large amplitude energy levels between the two limits of a rigid C_s(I) equilibrium structure and a rigid C_{2v} equilibrium structure. This correlation is made through the rotation and large amplitude energies of the nonrigid molecule that tunnels through all C_s(I), C_s(II) and C_{2v} versions.

A version of the C_{2v} structure is shown in Fig. 4, and in Table 4 we show the appropriate $C_{2v}(M)$ molecular symmetry group for this structure, if we presume it not to undergo observable tunneling to other minima. A symmetry coordinate that approximately describes the flip vibration is

$$S_{\text{flip}} = \angle H_1CH_2 - \angle H_3CH_2, \tag{4}$$

and it has B_2 symmetry in $C_{2v}(M)$. The asymmetric top states $J_{K_aK_c}$ have symmetries as given in Table 5, which is the same as the situation for the formaldehyde molecule (see Table 12-9 in Ref. [23]).

Table 4
The molecular symmetry group $C_{2v}(M)$ for the version of the C_{2v} structure shown in Fig. 4

$C_{2v}(M)$:	E	(13)(45)	(45)*	(13)*
C_{2v} :	E	C_{2a}	σ_{ab}	σ_{ac}
Equiv. rot.:	R^0	R_a^π	R_c^π	R_b^π
A_1 :	1	1	1	1
A_2 :	1	1	−1	−1
B_1 :	1	−1	−1	1
B_2 :	1	−1	1	−1

Table 5
The symmetry of the asymmetric top wavefunctions in the group $C_{2v}(M)$ as a function of the evennes (e) and oddness (o) of K_a and K_c

K_aK_c	Symmetry
ee	A_1
eo	A_2
oe	B_2
oo	B_1

Table 6
The correlation table giving the representations of G_{240} induced by the irreducible representations of $C_{2v}(M)$

$C_{2v}(M)$	G_{240}
A_1	$A_1^+ + A_2^- + 2G_1^+ + 2G_2^- + 2H_1^+ + 2H_2^- + H_1^- + H_2^+ + I^+ + I^-$
A_2	$A_1^- + A_2^+ + 2G_1^- + 2G_2^+ + 2H_1^- + 2H_2^+ + H_1^+ + H_2^- + I^- + I^+$
B_1	$G_1^+ + G_1^- + G_2^+ + G_2^- + H_1^+ + H_1^- + H_2^+ + H_2^- + 2I^+ + 2I^-$
B_2	$G_1^- + G_1^+ + G_2^- + G_2^+ + H_1^- + H_1^+ + H_2^- + H_2^+ + 2I^- + 2I^+$

The molecular symmetry group for the nonrigid molecule that tunnels through all C_s(I), C_s(II) and C_{2v} versions is the group $G_{240} = S_5 \otimes \{E, E^*\}$ as discussed in Ref. [16]. The correlation table giving the representations of G_{240} induced by the representations of $C_{2v}(M)$ (See Section 5.9.1 of Ref. [23]) are given in Table 6. If we add the nuclear spin statistical weights, and omit all the missing levels, we get the correlations shown in Table 7. Using these results, we can determine the symmetries in $C_{2v}(M)$ and G_{240} of the rotation-flip energy levels of the rigid C_{2v} molecule and four of these are given in Table 8.

A version of the C_s(I) structure is shown in Fig. 5, and in Table 9 we show the appropriate $C_s(M)$ molecular symmetry group for this structure, if we presume it not to undergo observable tunneling to other minima. The torsional vibrational coordinate has A'' symmetry, and the asymmetric top states $J_{K_aK_c}$ have symmetry A' or A'' as K_c is even or odd, respectively. If there is observable tunneling through the C_s(II) structure, the MS group enlarges to become the G_{12} group as discussed in Ref. [16] (see Table A-24 in Ref. [23]). When there is significant internal rotation tunneling, the successive internal rotation states are labeled using the internal rotation quantum number K_i. Further tunneling through the C_{2v} structure leads to labeling using the G_{240} MS group. The correlation of the symmetry species of the G_{12} and G_{240} groups is discussed in Ref. [16].

Table 7
The correlation table for G_{240} and $C_{2v}(M)$ with nuclear spin statistical weights added

$C_{2v}(M)$	G_{240}
$A_1(20)$	$A_2^-(6) + 2G_2^-(4) + 2H_2^-(2) + H_2^+(2)$
$A_2(20)$	$A_2^+(6) + 2G_2^+(4) + 2H_2^+(2) + H_2^-(2)$
$B_1(12)$	$G_2^+(4) + G_2^-(4) + H_2^+(2) + H_2^-(2)$
$B_2(12)$	$G_2^-(4) + G_2^+(4) + H_2^-(2) + H_2^+(2)$

Only states with nonzero statistical weights are included.

Table 8
Symmetries of rotation-flip levels of non-tunneling C_{2v} CH_5^+ in the molecular symmetry groups $C_{2v}(M)$ and G_{240}

v_{flip}	$J_{K_aK_c}$	$C_{2v}(M)$	G_{240}
1	1_{01}	$B_1(12)$	$G_2^+(4) + G_2^-(4) + H_2^+(2) + H_2^-(2)$
1	0_{00}	$B_2(12)$	$G_2^-(4) + G_2^+(4) + H_2^-(2) + H_2^+(2)$
0	1_{01}	$A_2(20)$	$A_2^+(6) + 2G_2^+(4) + 2H_2^+(2) + H_2^-(2)$
0	0_{00}	$A_1(20)$	$A_2^-(6) + 2G_2^-(4) + 2H_2^-(2) + H_2^+(2)$

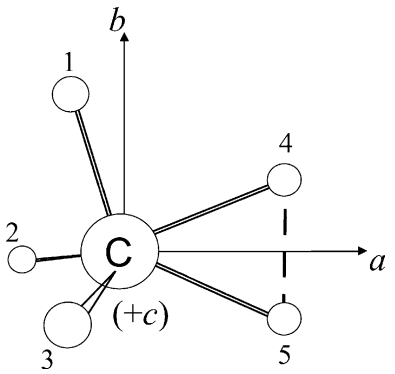

Fig. 5. A version of the C_s(I) structure.

The correlation table for the symmetry species of the groups $C_s(M) \rightarrow G_{12} \rightarrow G_{240}$, with statistical weights added, and using the quantum number K_i, are given in Table 10 starting from four rotation–torsion states of the rigid C_s(I) molecule. Each rotation–torsion state of the rigid $C_s(M)$ molecule is split into four levels by internal rotation tunneling, two of A symmetry and two of E symmetry in G_{12}. The splitting between the $K_i = 3$ (lower) and 3 (upper) levels is proportional to the internal rotation barrier height, and in the event of a zero barrier the internal rotation energies for each rotational level are proportional to K_i^2. Each rotation–internal rotation level of the G_{12} molecule is further split by the flip tunneling to give the G_{240} symmetry species shown in the right hand column of Table 10.

We can combine the correlations given in Tables 8 and 10 for each rotational state of the molecule to allow for large amplitude motions encompassing the C_s(I), C_s(II) and C_{2v} structures. In Fig. 6, this is done for the 0_{00} rotational level, where the central ladder of 10 energy levels shows the tunneling fine structure when there is tunneling through all three low energy structures; for each of the 10 levels we give the G_{240} symmetry label, and the nuclear spin statistical weight (in parentheses). Moving from the left to the central levels of Fig. 6 follows the bottom quarter of Table 10 and represents the energy levels for three situations: (a) C_s, in which the molecule rigidly has the C_s(I) structure with no observable tunneling splittings, (b) $C_s \rightarrow G_{12}$, in which the C_s(II) structure is close to the C_s(I) structure in energy (but the C_{2v} structure is high in energy) so that there is internal rotation tunneling splitting of each level into four levels labeled in the low barrier situation using the internal rotation quantum number K_i, and (c) $G_{12} \rightarrow G_{240}$, where we have

Table 9
The molecular symmetry group $C_s(M)$ for the version of the C_s(I) structure shown in Fig. 5

$C_s(M)$:	E	$(23)^*$
C_s :	E	σ_{ab}
Equiv. rot.:	R^0	R_c^π
A' :	1	1
A'' :	1	−1

Table 10
The correlation of the symmetries of the rotation–torsion energy levels of non-tunneling C_s(I) CH_5^+ in the molecular symmetry group $C_s(M)$, with the tunneling internal rotation states (labeled by K_i) using the groups G_{12} and G_{240}

$J_{K_aK_c}$	v_{tor}	$C_s(M)$	K_i	G_{12}	G_{240}
1_{01}	1	$A'(32)$	6(lower)	$A_1'(4)$	$G_2^-(4)$
			5	$E''(12)$	$G_2^+(4) + G_2^-(4) + H_2^+(2) + H_2^-(2)$
			4	$E'(4)$	$H_2^+(2) + H_2^-(2)$
			3(upper)	$A_1''(12)$	$A_2^-(6) + G_2^-(4) + H_2^-(2)$
	0	$A''(32)$	3(lower)	$A_2''(12)$	$A_2^+(6) + G_2^+(4) + H_2^+(2)$
			2	$E'(4)$	$H_2^+(2) + H_2^-(2)$
			1	$E''(12)$	$G_2^+(4) + G_2^-(4) + H_2^+(2) + H_2^-(2)$
			0	$A_2'(4)$	$G_2^+(4)$
0_{00}	1	$A''(32)$	6(lower)	$A_2'(4)$	$G_2^+(4)$
			5	$E''(12)$	$G_2^+(4) + G_2^-(4) + H_2^+(2) + H_2^-(2)$
			4	$E'(4)$	$H_2^+(2) + H_2^-(2)$
			3(upper)	$A_2''(12)$	$A_2^+(6) + G_2^+(4) + H_2^+(2)$
	0	$A'(32)$	3(lower)	$A_1''(12)$	$A_2^-(6) + G_2^-(4) + H_2^-(2)$
			2	$E'(4)$	$H_2^+(2) + H_2^-(2)$
			1	$E''(12)$	$G_2^+(4) + G_2^-(4) + H_2^+(2) + H_2^-(2)$
			0	$A_1'(4)$	$G_2^-(4)$

The statistical weights are given in parentheses.

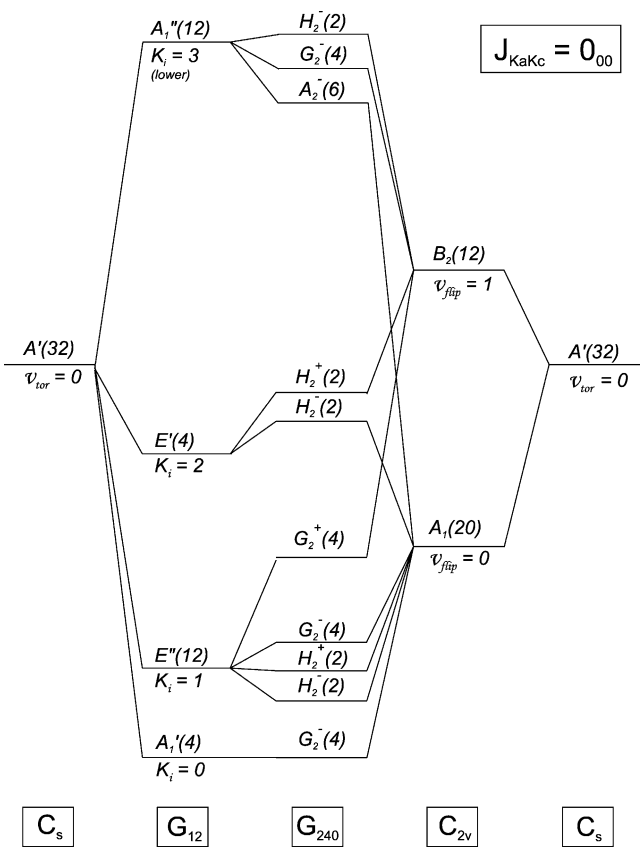

Fig. 6. The correlation of the 0_{00} energy level of the rigid C_s(I) structure, the internally rotating G_{12} structure, the fully nonrigid G_{240} structure, and the rigid C_{2v} structure.

included the effect of flip-tunneling. Alternatively, moving from the right to the central levels, Fig. 6 represents the energy levels for three situations: (a) C_s where the molecule rigidly has the C_s(I) structure with no observable tunneling splitting as on the left of the diagram, (b) $C_s(\mathrm{I}) \rightarrow C_{2v}$, where now the C_{2v} structure is close to the C_s(I) structure in energy (but the C_s(II) structure is high in energy) so that there is a flip tunneling splitting of each level into two (with a flip barrier of $300\ \mathrm{cm}^{-1}$ this splitting is calculated to be $1.5\ \mathrm{cm}^{-1}$; if the C_{2v} structure is the lowest energy structure with the C_s(I) and C_s(II) structures high then this splitting would represent the flip fundamental vibration of the C_{2v} structure), and (c) $C_{2v} \rightarrow G_{240}$ (from Table 8), where the effect of internal rotation tunneling is included.

In Fig. 6, the order of the energy levels in the G_{240} situation is taken from the numerical results for $J = 0$ in Table 5 of Ref. [19]. Similar diagrams can be drawn for higher 0_{00} levels involving the $v_{tor} = 1$, and the $v_{flip} = 2$ and 3 states. For the 1_{01} rotational level, a very similar correlation diagram to that given in Fig. 6 is obtained, but the symmetry species must be changed from those given for the 0_{00} level, according to the rules: $' \leftrightarrow ''$ for C_s, $1 \leftrightarrow 2$ for C_{2v} and G_{12}, and $+ \leftrightarrow -$ for G_{240}. Allowed rotation–vibration transitions are connected by A'' for C_s, A_2 for C_{2v}, A_2' for G_{12} and A_1^- for G_{240}. This means that the large amplitude fine structure for the $1_{01} \leftarrow 0_{00}$ transition will involve transitions between levels that are in the same position in the fine structure ladder of each of the two rotational states, i.e. the allowed transitions between the two sets of large amplitude fine structure levels will be from the bottom level of 0_{00} to the bottom level of 1_{01}, second-to-second,…, top-to-top. Thus, the fine structure line splittings in the spectrum of the $1_{01} \leftarrow 0_{00}$ transition will reflect the difference between the energy level splittings in the 1_{01} and 0_{00} rotational states, and this arises from the difference in the effective large amplitude potential energy function for the two rotational states; presumably this difference will be small. The same situation obtains for all rotational transitions.

5. Simulation of the rotational spectrum

To simulate the absorption spectrum with absolute intensities, it is necessary to calculate the partition function. For this purpose, sufficient accuracy is obtained if we use an 'uncoupled' free-rotor approximation and take the rotation–vibration energies as the sum of E_{rot}, E_{introt}, E_{flip} and E_{vib}, where

$$E_{rot}/\mathrm{cm}^{-1} = 7.575\, J(J+1) + 0.682\, K^2 \quad (5)$$

in the symmetric top approximation, and

$$E_{introt}/\mathrm{cm}^{-1} = 35.4\, K_i^2, \quad (6)$$

in the free internal rotor approximation, where $K_i = 0, 1, 2,\ldots$ is the internal rotation quantum number. The flip

Table 11
The wavenumber (in cm^{-1}) of the 1D flip motion energy levels used in the calculation of the partition function

v_{flip}	E	flip	E
0	(109.3)[a]	11	1355.3
1	1.5	12	1541.0
2	168.2	13	1733.8
3	206.4	14	1933.3
4	317.7	15	2139.2
5	426.7	16	2351.2
6	555.2	17	2569.0
7	695.4	18	2792.2
8	846.6	19	3020.8
10	1177.3		

[a] The zero point energy in parentheses.

energies E_{flip} are taken as the numerically determined energies obtained, as described in Ref. [17], by solving the 1D Schrödinger equation for the flip-motion. For a flip barrier of 300 cm^{-1} these energies are given in wavenumber units (cm^{-1}) in Table 11. The vibrational energies E_{vib} are taken as the average of the scaled ab initio harmonic vibrational wavenumbers of the C_s(I) and C_s(II) structures given in Tables VII and VIII of Ref. [5]. We increased the upper energy level (E_{max}) used in calculating the partition function until convergence was obtained; for $T = 300$ K E_{max} was 2600 cm^{-1}, and for $T = 77$ K E_{max} was 600 cm^{-1}. In calculating the partition function, we must include the nuclear spin degeneracy; states of ($'$) species in G_{12} have a nuclear spin degeneracy of four, and those of ($''$) species have a nuclear spin degeneracy of 12. In this uncoupled free-rotor approximation, we determine that the partition function is 2350 at 77 K, and 52,250 at 300 K.

To calculate the line positions in the rotation spectrum, with large amplitude vibration fine structure, we use the 120 × 120 matrix approach, as described in Section IV of

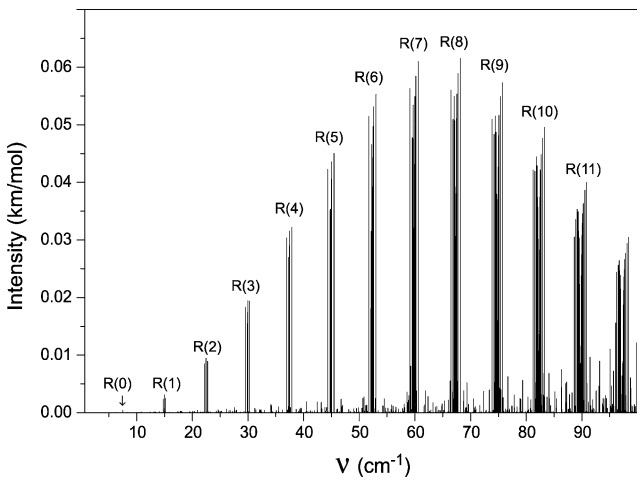

Fig. 7. Simulations at 300 K of the absorption spectrum. This simulation uses large amplitude energies obtained from the 120 × 120 matrix diagonalization under the assumption that the energies of the C_s(II) and C_{2v} structures are 30 and 300 cm^{-1}, respectively, above the energy of the C_s(I) structure.

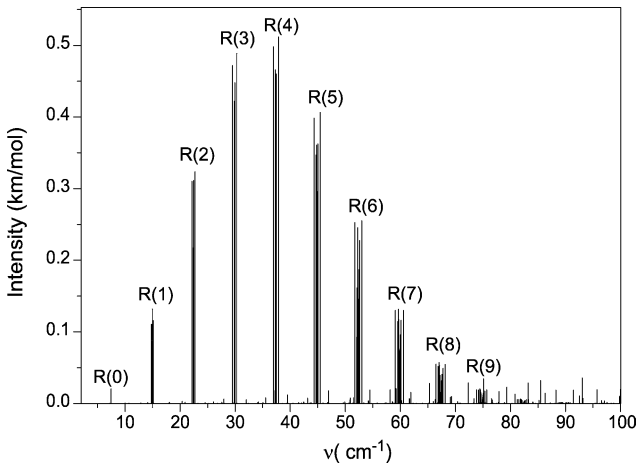

Fig. 8. Simulations at 77 K of the absorption spectrum. This simulation uses large amplitude energies obtained from the 120 × 120 matrix diagonalization under the assumption that the energies of the C_s(II) and C_{2v} structures are 30 and 300 cm^{-1}, respectively, above the energy of the C_s(I) structure.

Ref. [17], to calculate the rotational-large amplitude energy levels. Such energy level calculations were made before in Ref. [19] where we used three different ab initio potentials. As the starting point in the present paper, we use the results from Ref. [19] obtained using the optimized geometries and 'bare' ab initio potential from Ref. [5]. This potential has the C_s(II) structure at an energy of 30 cm^{-1}, and the C_{2v} structure at an energy of 300 cm^{-1}, both relative to the energy of the C_s(I) structure. Using these energy levels, and a dipole moment of 1.6 D for the C_s(I), C_s(II) and C_{2v} structures, we simulate the absorption spectrum of the molecule at temperatures of 300 and 77 K; the results are given in Figs. 7 and 8, respectively. A close up of the $R(0)$ transitions at 77 K is given in Fig. 9 to show the internal rotation fine structure.

The simulations are made with the assumption that the effective barrier to flip tunneling is the same in all rotational

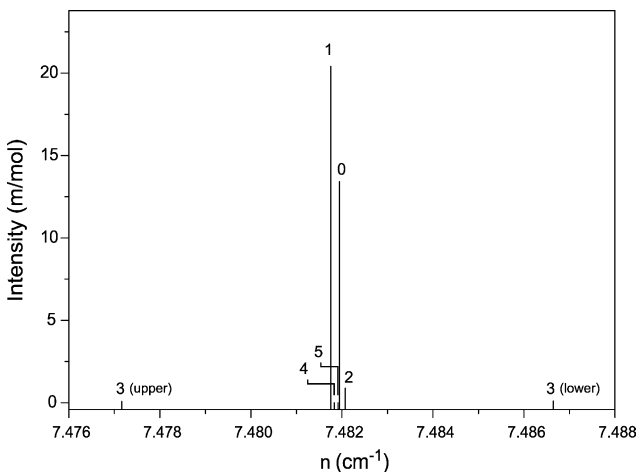

Fig. 9. Enlargement of the $R(0)$ spectrum from Fig. 8 at 77 K. The internal rotation fine structure is labeled by the K_i quantum number, and allowed transitions have $\Delta K_i = 0$.

levels, and as a result there are no line splittings due to flip tunneling.

We now focus on the $J = 1 \leftarrow 0$ rotational transition. If the molecule were rigidly C_s(I), C_s(II) or C_{2v} the $J = 1 \leftarrow 0$ spectrum would be a single line. If the C_s(I) structure were the lowest in energy with a small flip barrier through the C_{2v} structure, but with an insuperable barrier to internal rotation, then the $J = 1 \leftarrow 0$ spectrum would be a doublet consisting of the $v_{\text{flip}} = 1 \leftarrow 1$ and $0 \leftarrow 0$ transitions with a nuclear spin statistical weight ratio of 12/20. Internal rotation tunneling would split the $v_{\text{flip}} = 1 \leftarrow 1$ transition into four lines with statistical weights in the ratio 2:4:2:4, and split the $v_{\text{flip}} = 0 \leftarrow 1$ transition into six lines with statistical weights in the ratio 6:2:4:2:2:4. These results follow from the $C_s \rightarrow C_{2v} \rightarrow G_{240}$ correlation given in Fig. 6.

In Table 12, we give the internal-rotation flip energy levels for the molecule in the 0_{00} state for various values of the effective internal rotation and flip barriers; we choose values near the pure ab initio values of 30 and 300 cm^{-1} for the barriers. In Table 13, we present the results of calculating the fine structure of the $J = 1_{01} \leftarrow 0_{00}$ spectrum for an effective barrier to internal rotation of 50 cm^{-1} in both the 1_{01} and 0_{00} states. We show the fine structure obtained if the effective flip barrier in the 1_{01} state is 345, 300 or 265 cm^{-1} (corresponding to flip tunneling splittings of 1.0, 1.5 and 2.0 cm^{-1}, respectively), with the effective flip barrier in the 0_{00} state being held fixed at 300 cm^{-1}. The flip fine structure in the $J = 1_{01} \leftarrow 0_{00}$ spectrum is only sensitive to the difference in the flip tunneling splitting between the 1_{01} and 0_{00} states, and not to its actual value in the two states. The relative intensities of the fine structure lines split by the flip tunneling are given by the statistical

Table 12
The rotation internal–rotation flip energy levels E_{rirf} for the 0_{00} state for different values of the effective barriers to internal rotation and to the flip

ΔE_{flip} [a]	K_i	H_{ir} [b]		
		0	50	100
0[c]	3(lower)	328.3	316.6	304.7
	2	146.1	145.9	145.3
	1	36.5	36.5	36.4
	0	0.0	0.0	0.0
1.5[d]	3(lower)	328.7	316.9	304.9
		328.3	316.5	304.6
		327.7	315.9	303.9
	2	146.5	146.3	145.7
		145.7	145.5	144.9
	1	37.3	37.2	37.2
		36.3	36.2	36.2
		36.1	36.1	36.0
		35.9	35.9	35.8
	0	−0.4	−0.4	−0.4
3.6[e]	3(lower)	329.0	317.3	305.3
		328.1	316.4	304.4
		326.6	314.9	302.9
	2	147.0	146.8	146.2
		145.2	145.0	144.0
	1	38.3	38.3	38.2
		35.9	35.9	35.8
		35.6	35.6	35.5
		35.0	35.0	34.9
	0	−0.9	−0.8	−0.9
9.6[f]	3(lower)	330.1	318.4	306.4
		327.7	316.0	304.0
		323.6	311.9	299.9
	2	148.7	148.5	147.9
		143.6	143.4	142.8
	1	41.3	41.3	41.2
		35.1	35.1	35.0
		33.9	33.9	33.8
		32.5	32.5	32.4
	0	−2.6	−2.5	−2.6

[a] The splitting between the $v_{\text{flip}} = 1$ and 0 levels in the 1D flip model.
[b] The effective internal rotation barrier. This is the energy difference C_s(II)−C_s(I).
[c] Corresponding to an insuperable barrier to the flip. The barrier to the flip is the energy difference $C_{2v} - C_s$(I).
[d] Corresponding to an effective barrier of 300 cm^{-1} to the flip.
[e] Corresponding to an effective barrier of 200 cm^{-1} to the flip.
[f] Corresponding to an effective barrier of 100 cm^{-1} to the flip.

Table 13
The rotation internal–rotation flip energy levels E_{rirf} in cm^{-1} for the 1_{01} state, and the wavenumbers of the internal–rotation flip fine structure ν in cm^{-1} for the 1_{01}–0_{00} rotational transition assuming an effective barrier of 300 cm^{-1} for the flip in the 0_{00} state

K_i	g_{ns} [a]	ΔE_{flip} [b]					
		1.0[c]		1.5[d]		2.0[e]	
		E_{rirf}	ν	E_{rirf}	ν	E_{rirf}	ν
3(lower)	2	324.30	7.40	324.38	7.49	324.47	7.57
	4	324.05	7.53	324.01	7.49	323.97	7.45
	6	323.63	7.74	323.38	7.49	323.13	7.24
2	2	153.62	7.36	153.74	7.48	153.87	7.61
	2	153.11	7.61	152.99	7.48	152.86	7.36
1	4	44.47	7.23	44.72	7.48	44.97	7.73
	4	43.80	7.56	43.72	7.48	43.64	7.40
	2	43.72	7.61	43.59	7.48	43.46	7.35
	2	43.55	7.69	43.34	7.48	43.13	7.27
0	4	7.23	7.61	7.10	7.48	6.97	7.35

The effective internal rotation barrier. (i.e. the energy difference C_s(II)−C_s(I)) is taken to be 50 cm^{-1} in the 1_{01} and 0_{00} states.
[a] The nuclear spin statistical weight.
[b] The splitting between the $v_{\text{flip}} = 1$ and 0 levels in the 1D flip model.
[c] Corresponding to an effective barrier of 345 cm^{-1} to the flip in the 1_{01} state. The barrier to the flip is the energy difference $C_{2v} - C_s$(I).
[d] Corresponding to an effective barrier of 300 cm^{-1} to the flip in the 1_{01} state.
[e] Corresponding to an effective barrier of 265 cm^{-1} to the flip in the 1_{01} state.

weights. In the event that the splitting by flip tunneling is resolved the single $K_i = 0 \leftarrow 0$ line, which is not split by flip tunneling, will be the most intense fine structure line at 77 K, with an intensity of 13 m/mol.

The aim of these calculations is to present the possible patterns of the large amplitude fine structure, both for the rotational energy levels (Table 12) and for the $J = 1_{01} \leftarrow 0_{00}$ spectrum (Table 13). As higher rotation–vibration levels are probed spectroscopically, the effect of the tunneling of versions of the C_s(II) structure through versions of the C_{4v} structure (number 4 in Fig. 1) will next have to be considered.

Acknowledgements

We are very grateful to T. Carrington Jr., A.L.L. East, and J.K.G. Watson for critically reading the first draft of the manuscript. At our request T.J. Sears made calculations of the rotation–torsion spectrum using the computer code he developed for C_2H_5 in order to check our calculations. We are very grateful to him for this.

References

[1] V.L. Talroze, A.K. Lyubimova, Dokl. Akad. Nauk SSSR. 86 (1952) 909.
[2] A.J.R. Heck, L.J. de Koning, N.M.M. Nibbering, J. Am. Soc. Mass Spectrom. 26 (1991) 453.
[3] G.A. Olah, G. Rasul, Acc. Chem. Res. 30 (1997) 245.
[4] P.v.R. Schleyer, J.W.de M Carneiro, J. Comput. Chem. 13 (1992) 997.
[5] P.R. Schreiner, S.-J. Kim, H.F. Schaefer, P.v.R. Schleyer, J. Chem. Phys. 99 (1993) 3716.
[6] H. Müller, W. Kutzelnigg, J. Noga, W. Klopper, J. Chem. Phys. 106 (1997) 1863.
[7] C.M. Gabrys, D. Uy, M.-F. Jagod, T. Oka, T. Amano, J. Phys. Chem. 99 (1995) 15611.
[8] P.C. Gomez, P.R. Bunker, Chem. Phys. Lett. 165 (1990) 351.
[9] E.T. White, J. Tang, T. Oka, Science 284 (1999) 135.
[10] H. Bogey, H. Bolvin, M. Cordonnier, C. Demuynck, J.L. Destombes, R. Escribano, P.C. Gomez, Can. J. Phys. 72 (1994) 967.
[11] R.G.A. Bone, T.W. Rowlands, N.C. Handy, A.J. Stone, Mol. Phys. 72 (1991) 33.
[12] P.R. Bunker, T. Carrington Jr., P.C. Gomez, M.D. Marshall, M. Kofranek, H. Lischka, A. Karpfen, J. Chem. Phys. 91 (1989) 5154.
[13] J.T. Hougen, P.R. Bunker, J.W.C. Johns, J. Mol. Spectrosc. 34 (1970) 136.
[14] J.C.D. Brand, Ch.V.S. Rao, J. Mol. Spectrosc. 61 (1976) 360.
[15] M. Kreglewski, J. Mol. Spectrosc. 72 (1978) 1.
[16] P.R. Bunker, J. Mol. Spectrosc. 176 (1996) 297.
[17] M. Kolbuszewski, P.R. Bunker, J. Chem. Phys. 105 (1996) 3649.
[18] A.L.L. East, P.R. Bunker, J. Mol. Spectrosc. 183 (1997) 157.
[19] A.L.L. East, M. Kolbuszewski, P.R. Bunker, J. Phys. Chem. A 101 (1997) 6746.
[20] MOLPRO is a package of ab initio programs written by H.-J. Werner and P.J. Knowles, with contributions from R.D. Amos, A. Bernhardsson, A. Berning, P. Celani, D.L. Cooper, M.J.O. Deegan, A.J. Dobbyn, F. Eckert, C. Hampel, G. Hetzer, T. Korona, R. Lindh, A.W. Lloyd, S.J. McNicholas, F.R. Manby, W. Meyer, M.E. Mura, A. Nicklass, P. Palmieri, R.M. Pitzer, G. Rauhut, M. Schütz, H. Stoll, A.J. Stone, R. Tarroni, and T. Thorsteinsson.
[21] T.H. Dunning Jr., J. Chem. Phys. 90 (1989) 1007.
[22] M.J. Frisch, G.W. Trucks, H.B. Schiegel, G.E. Scuseria, M.A. Robb, J.R. Cheeseman, V.G. Zakrzewski, J.A. Montgomery, Jr., R.E. Stratmann, J.C. Burant, S. Dapprich, J.M. Millam, A.D. Daniels, K.N. Kudin, M.C. Strain, O. Farkas, J. Tomasi, V. Barone, M. Cossi, R Cammi, B. Mennucci, C. Pomelli, C. Adamo, S. Clifford, J. Ochterski, G.A. Petersson, P.Y. Ayala, Q. Cui, K. Morokurna, D.K. Malick, A.D. Rabuck, K. Raghavachari, J.B. Foresman, J. Cioslowski, J.V. Ortiz, A.G. Baboul, B.B. Stefanov, G. Liu, A. Liashenko, P. Piskorz, I. Komaromi, R. Gomperts, R.L. Martin, D.J. Fox, T. Keith, M.A. Al-Laham, C.Y. Peng, A. Nanayakkara, M. Challacombe, P.M.W. Gill, B. Johnson, W. Chen, M.W. Wong, J.L. Andres, C. Gonzalez, M. Head-Gordon, E.S. Replogle, J.A. Pople, GAUSSIAN 98, Revision A.9, Gaussian, Inc., Pittsburgh PA, 1998.
[23] P.R. Bunker, P. Jensen, Molecular Symmetry and Spectroscopy, second ed., NRC Research Press, Ottawa, 1998, See http://www.nrc.ca/cisti/journals/mgraphs.html.